Study on Silicon Device of Microrobot System for Heterogeneous Integration

Ken Saito[1,2], Daniel S. Contreras[3], Yudai Takeshiro[4], Yuki Okamoto[4], Yuya Nakata[5], Taisuke Tanaka[5], Satoshi Kawamura[5], Minami Kaneko[1], Fumio Uchikoba[1], Yoshio Mita[4], and Kristofer S. J. Pister[3]

[1] *Department of Precision Machinery Engineering, College of Science and Technology, Nihon University, Funabashi-shi, Chiba 274 Japan*
[2] *Department of Mechanical Engineering, University of California, Berkeley, CA 94720, USA*
[3] *Department of Electrical Engineering and Computer Sciences, University of California, Berkeley, CA 94720, USA*
[4] *Department of Electrical Engineering and Information Systems, The University of Tokyo, Bunkyo-ku, Tokyo 113, Japan*
[5] *Precision Machinery Engineering, Graduate School of Science and Technology, Nihon University, Chiyoda-ku, Tokyo, 101 Japan*

***Abstract*—The ideal microrobots are millimeter sized with integrated actuators, power sources, sensors, and controllers. Many researchers take the inspiration from insects for the mechanical or electrical designs to construct small sized robotic systems. Previously, the authors proposed and demonstrated microrobots which can replicate the tripod gait locomotion of an ant and the legs were actuated by shape memory alloy actuators. Shape memory alloy provided a large deformation and a large force, but the power consumption was as high as 94 mW to actuate a single leg. This paper discusses the silicon electrostatic inchworm motor chip with low energy consumption for the robot leg by using a small-size power source. The inchworm motor chip has actuated by electrostatic motors. The power consumption is low as 1.0 mW compering with shape memory alloy actuators. The reciprocal motion of the inchworm motor chip is power by the silicon photovoltaic cells. Results show the 7.5 mm square size photovoltaic cells could produce 60 V to actuate the inchworm motor chip. The generated force is enough to move the leg of the microrobot. We have shown actuation of the microrobot leg using an electrostatic inchworm motor chip. This result is the first instance of an electrostatic motor driving an off-chip structure.**

Keywords—heterogeneous integration; silicon device; microrobot; electrostatic motor; photovoltaic cells

I. INTRODUCTION

Several microrobot systems from the micrometer to centimeter scale have been demonstrated [1-12]. Among these demonstrations, the micrometer scale ones have potential usages in special environments such as surgery inside the narrow blood vessel of a human brain or micro assembly for the small size mechanical system [4, 8] but it is difficult to add power sources and controllers into the microscale system. Therefore, passive control schemes by external electrical or magnetic forces are commonly implemented. On the other hand, a lot of centimeter-size robots have been constructed by the miniaturizations of electrical components with integrated sensors, actuators, power sources and controllers [6, 9]. Despite the fact that multiple bio-inspired robots have been proposed, millimeter scale robots do not perform like insects due to the difficulty in integrating power sources and actuators onto the robot [13, 14]. In particular, the locomotion mechanisms of insects attract the attention of researchers [5, 7]. In seeking further miniaturization, some researchers use micro fabrication technology to fabricate small sized actuators [15, 16]. For example, piezoelectric actuators, shape memory alloy actuators, electrostatic actuators, ion-exchange polymer actuators, and so on are a few examples. These actuators have different strengths, such as power consumption, switching speed, force generation, displacement, and fabrication difficulty. In general, an actuator can only generate either rotary or linear motion and mechanical mechanisms are necessary to convert the movements generated by the actuators to locomotion.

Previously, the authors have shown a millimeter scale hexapod-type microrobot to perform the tripod gait locomotion of an ant [17], and a quadruped-type microrobot to replicate the quadrupedal gait locomotion of an animal [18] by using shape memory alloy actuators for large deformation and large force. This paper discusses the electrostatic inchworm motor chip [19-21] with low energy consumption using a small size power source. The leg of the microrobot is designed to allow reciprocal motions and powered by silicon photovoltaic (hereafter PV) cells [22, 23].

II. HIGH-VOLTAGE SILICON PHOTOVOLTAIC CELLS

Fig. 1 shows the fabricated high-voltage Silicon PV cell array. The PV cell array was designed in an area of 7.5 mm square. The device was made by CMOS post-process dry release and device isolation method. The array consists of 144 PV cells connected in series and each cell has a p-diffusion layer on n-well. The details of the design and process method are shown in reference [22, 23].

Fig. 2 shows the I-V characteristics of the PV cell array. The measurement of the PV cell array was conducted using the KEITHLEY 2000 MULTIMETER. The light source was a 54 LED array (6 W) with DC 6 V voltage source. The open circuit voltage (V_{OC}) was 69 V, from which we can deduce that the open circuit voltage of each cell was about 0.48 V on average. The short circuit current (I_{SC}) was 28 μA. The maximum power (P_{MAX}) was 1.1 mW, where the voltage was 50 V and the current was 22 μA. The I_{SC} depends on light intensity, therefore, changing the light source to more high light intensity will increase the I_{SC}.

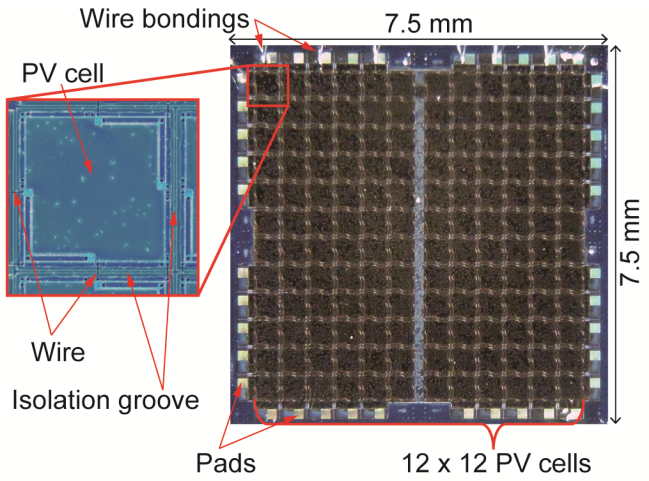

Fig. 1. High-voltage silicon PV cell array.

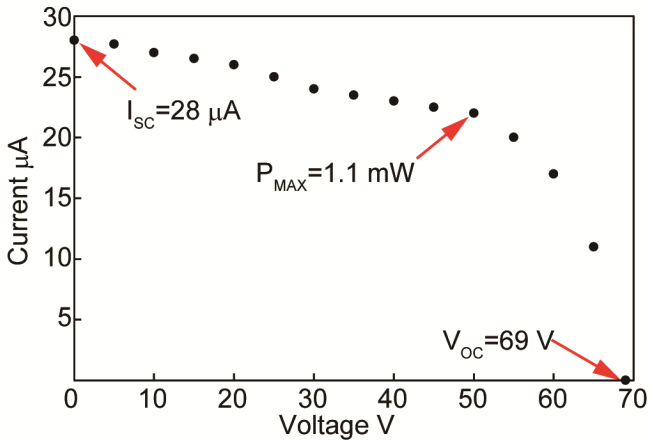

Fig. 2. I-V curve of Silicon PV array.

III. Electrostatic Motors

As an alternative low-power means of actuation, electrostatic inchworm motors can be used to drive the legs of the microrobot. MEMS electrostatic inchworm motors are based on capacitively driven gap-closing actuators (GCA) working in tandem to displace a shuttle linearly at over 100 µN force output without any static current [19].

Fig. 3 shows an inchworm motor chip. The authors used an angled-arm design based on work from [20]. In this design, the GCAs use an attached angled-arm to impact a central shuttle and move it in a preferential direction. The motors have a gapsize of 2.1 µm and each step of the motor moves the shuttle by 1 µm. Each GCA has 70 fingers, totaling 140 fingers for each actuation step. The inchworm motor chiplet measures a total area of approximately 2.2 mm x 2.5 mm. The electrostatic inchworm motors are fabricated in a 3-mask silicon-on-insulator (SOI) process. The SOI wafers had a 40 µm device layer, 2 µm buried oxide, and 550 µm handle wafer. A layer of 100 nm-thick aluminum is deposited on the device-layer silicon to define the contact pads. The device layer silicon is etched to

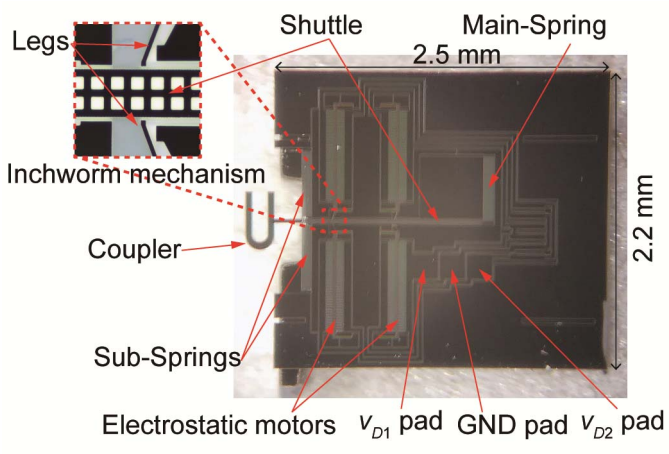

Fig. 3. Fabricated inchworm motor chip.

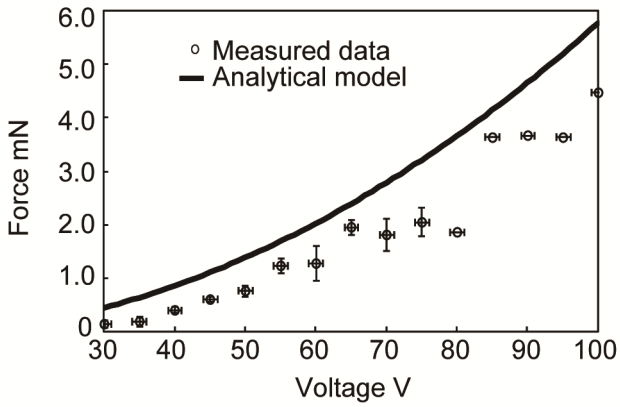

Fig. 4. The raw force output of the inchworm motor chip.

form the structure of the motors using DRIE. A backside etch is then performed to reduce the mass and release the singulated chiplets from the substrate.

Figure 4 shows the force output of an electrostatic inchworm motor. Force measurements are taken using a serpentine spring assembly attached to the motor shuttle. The serpentine assembly has a spring constant of 18.5 N/m. By measuring the displacement of the inchworm shuttle, we can relate this to the force output of the motor. The solid line highlights the analytical calculation of the force output. We can see that at 60 V we get an average force output of over 1 mN from 5 measured devices. The original angled-arm inchworm motors shown in [20] were able to generate 1.9 mN at 110 V. Previous work has shown 0.50 mN of force at 60V [21] while the newly fabricated devices have demonstrated 1.3 mN of force at 60 V. Discrepancies between the analytical model and the measured values can be attributed to unaccounted lateral etching of the silicon sidewalls. This can increase the effective finger gap size and change the spring constants of the springs.

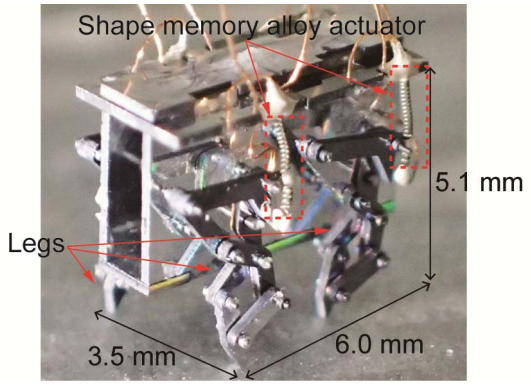

Fig. 5. Previous microrobot system using shape memory alloy actuator [18].

IV. Leg of the Microrobot System

Fig. 5 shows the previous quadruped-type microrobot using shape memory alloy actuators [18]. Each leg of the robot can perform the stepping motion via a single actuator. A shape memory alloy actuator is changed to electrostatic inchworm motors in this work. The leg is fixed on both sides of the body and the microrobot can increase the number of the legs easily. In this paper, the actuator connection part has been redesigned to accommodate the electrostatic inchworm motors.

Fig. 6 shows the mechanical parts of the leg made from a silicon wafer except the shaft and the steady pin. The shapes of the mechanical parts are machined by the inductively coupled plasma dry etching process with photolithography technology. The authors have manual assembled the mechanical parts of the robot because microfabrication technology is hard to construct the complicated three-dimensional structure. In the process, 200 μm-thick silicon wafers were used for the mechanical parts except the washer which used 100 μm-thick silicon wafers. The shaft was constructed by using 0.1 ± 0.002 μm in diameter cemented carbide. The washer was mounted to rigidly connected, the washer and the shaft were glued using cyanoacrylate. All silicon parts have a clearance of a 10 μm

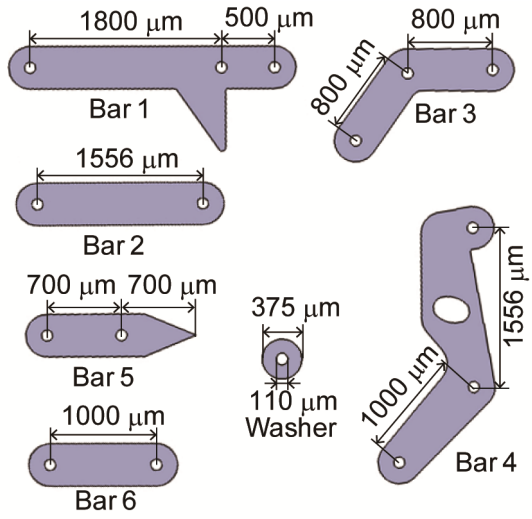

Fig. 6. Mechanical parts of the leg.

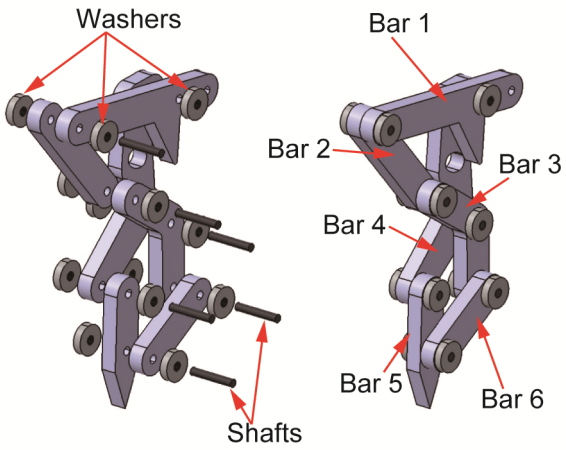

Fig. 7. Accembling method of the leg.

can only generate the rotary motion or linear motion, linkage assemblies are needed for a microrobot to move using the stepping pattern. The stepping pattern realized by two sets of four-bar linkages. Bar 1, bar 2, bar 3, and bar 4 are the primarily (top) four-bar linkage. Bar 3, bar 4, bar 5, and bar 6 are the secondly (bottom) four-bar linkage. The primarily four-bar linkage and secondly four-bar linkage are combined with each other with bar 3 and bar 4 (Fig. 7).

Fig. 8 shows the leg motion and trajectory of the leg. The (x_0, y_0) is the origin coordinate which is the only fix point to the body frame of the robot. The inflection point of the trajectory has four points such as (x_1, y_1), (x_2, y_2), (x_3, y_3), and (x_4, y_4). The steady pin and the hole of bar 4 cause the inflection of the

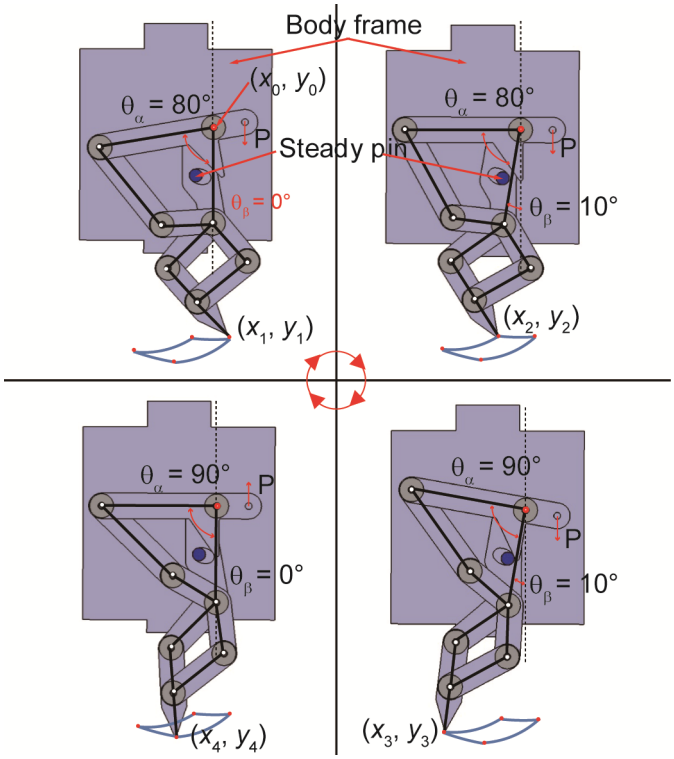

Fig. 8. Leg motion and trajectory of the leg.

TABLE I. DERIVED COORDINATES OF EACH FOOT POINT

Foot point	θ_α and θ_β	Coordinates (μm)
(x_1,y_1)	80° and 0°	(227.2, -3249.4)
(x_2,y_2)	80° and 10°	(-340.5, -3239.5)
(x_3,y_3)	90° and 10°	(-1248.6, -3440.3)
(x_4,y_4)	90° and 0°	(-632.3, -3604.9)

trajectory. The four points can be expressed by the difference of angles of θ_α and θ_β. The difference of θ_α and θ_β can perform the reciprocal movement of point P. In other words, Fig. 8 shows that the designed leg can perform the stepping motion by the reciprocal movement of point P.

Table 1 shows the derived coordinates of each foot point using the length between the each joint of the leg (Fig. 2), θ_α and θ_β. The coordinates were derived using trigonometric function. This result shows the designed leg can perform the stepping motion which is need to move the quadruped-type microrobot.

V. EXPERIMENTAL RESULTS

The anode-side of PV cell array was connected to the solid resistor at the collector of the transistor (Fig. 9). In other words, the generated voltage by the PV cell, V_{PV}, was used as the voltage source of the circuit. The Fluke 280 waveform generator was used for switching the transistor (2N5550) for generating the driving waveform v_{D1} and v_{D2} for the

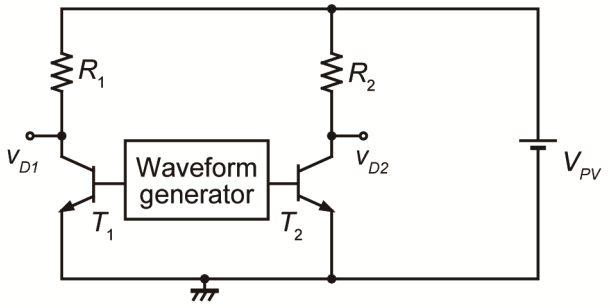

Fig. 9. Circuit diagram of driver circuit.

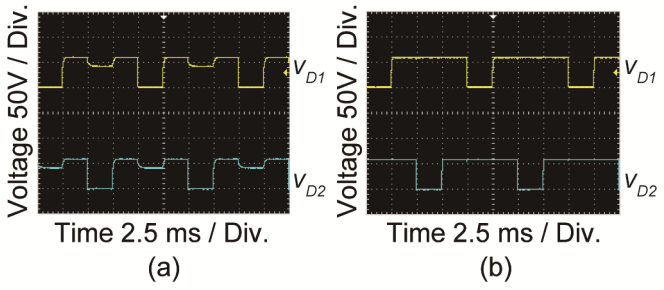

Fig. 10. Example of driving waveform.

electrostatic inchworm motors. The driving waveforms were two offset 60 V amplitude 50 Hz square waves, one for each of the GCAs of the motor. The circuit constant was R_1=R_2=2.2 MΩ.

Fig. 10 shows the example of the driving waveform of the electrostatic inchworm motor. Fig. 10 (a) is the driving waveform using PV cell array where Fig.10 (b) is the driving waveform using a voltage source. The driving waveform is square wave with pulse width 10 ms, pulse period 7.5 ms, pulse amplitude 60 V. Fig. 10 (a) shows the voltage drop off in the middle of the square wave. The voltage drop will increase in the case of changing to small R_1 and R_2 of driver circuit. In addition, the voltage drop also increase in the case of lower light intensity. This voltage drop can be avoid using more high light intensity light source (For example Xenon lamp).

Figure 11 shows the actuation of the leg using electrostatic inchworm motors. The coupler attached to the shuttle of the electrostatic inchworm motors was connected to the leg through the shaft of point P. The result in Figure 11 shows that the electrostatic inchworm motors produced about 250 μm in displacement to move the leg of the microrobot. However, the pull motion was not enough to actuate the leg from (x_4, y_4) to (x_1, y_1). This is because main-spring and sub-spring was designed to generate the 500 μN pull motion. The pull motion using spring structure is not realistic. The authors planning to design two electrostatic inchworm motors arranged to be opposed each other to generate the reciprocal motion.

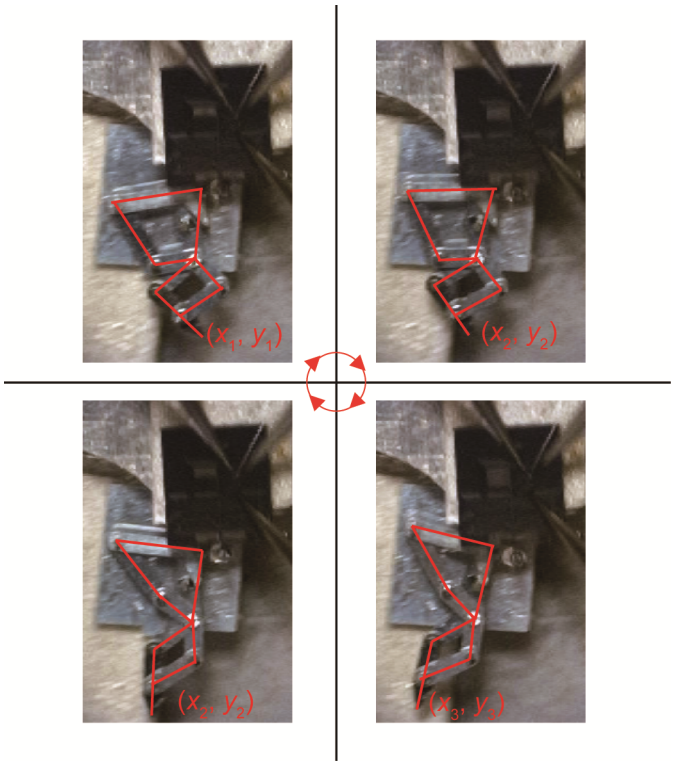

Fig. 11. Electrostatic inchworm motor for leg actuation.

VI. CONCLUSION

In this paper, the electrostatic actuator with low energy consumption is powered by a 7.5 mm x 7.5 mm Silicon photovoltaic cells with an output voltage of 60 Volts. The generated force of the electrostatic inchworm motors was enough to actuate the leg of the microrobot. The leg of the microrobot could move using the electrostatic inchworm motors with proper driving waveforms for large displacements. In the future, the authors will design the millimeter scale locomotive robot with silicon PV cell driven electrostatic inchworm motors.

ACKNOWLEDGMENT

The fabrication of the microrobot was supported by Research Center for Micro Functional Devices, Nihon University. Fabrication of the inchworm motors was supported by the UC Berkeley Marvell Nanofabrication Laboratory. The authors would like to acknowledge the Berkeley Sensor and Actuator Center and the UC Berkeley Swarm Lab for their continued support. VLSI Design and Education Center (VDEC), the University of Tokyo (UTokyo) and Phenitec Semiconductor are acknowledged for CMOS-SOI wafer fabrication. Japanese Ministry of Education, Sports, Culture, Science and Technology (MEXT) is acknowledged for financial support through Nanotechnology Platform to UTokyo VDEC used for PV cell post-process.

REFERENCES

[1] T. Ebefors, J.U Mattsson, E. Kälvesten, and G. Stemme, "A WALKING SILICON MICRO-ROBOT," Proc. of the 10th Int. Conference on Solid-State Sensors and Actuators, Sendai, Japan, 1999, pp 1202-1205.

[2] S. Hollar, A. Flynn, C. Bellew, and K.S.J. Pister, "Solar powered 10 mg silicon robot." Proc. of the IEEE The Sixteenth Annual International Conference on Micro Electro Mechanical Systems, Kyoto, Japan, 2002, pp. 706-711, 10.1109/MEMSYS.2003.1189847.

[3] J. Ryu, Y. Jeong, Y. Tak, B. Kim, B. Kim, and J. Park, "A ciliary motion based 8-legged walking micro robot using cast IPMC actuators." Proceedings of 2002 International Symposium on Micromechatronics and Human Science, 2002, pp. 85-91, 10.1109/MHS.2002.1058016

[4] B.R. Donald, C.G. Levey, C.D. McGray, I. Paprotny, and D. Rus, "An Untethered, Electrostatic, Globally Controllable MEMS Micro-Robot." Journal of Microelectromechanical Systems, 15(1), 2006, pp. 1-15, 10.1109/JMEMS.2005.863697.

[5] M.A. Hoover, E. Steltz, and S.R Fearing, "RoACH: An autonomous 2.4 g crawling hexapod robot." In Proceedings of the 2008 IEEE/RSJ International Conference on Intelligent Robots and Systems, Nice, France, 22–26 September 2008; pp. 26–33, 10.1109/IROS.2008.4651149.

[6] S. Kernbach, and O. Kernbach, "Collective energy homeostasis in a large-scale microrobotic swarm." Robotics and Autonomous Systems, 59, 2011, pp. 1090-1101, 10.1016/j.robot.2011.08.001.

[7] R.J. Wood, B. Finio, M. Karpelson, K. Ma, N.O. Pérez-Arancibia. P.S. Sreetharan, H. Tanaka, and J.P. Whitney, "Progress on "Pico" Air Vehicles." The International Journal of Robotics 31(11), 2012, pp. 1292-1302, 10.1177/0278364912455073

[8] B.R. Donald, C.G. Levey, I. Paprotny, and D. Rus, "Planning and control for microassembly of structures composed of stress-engineered MEMS microrobots." The International Journal of Robotics Research 32(2) 2013, pp. 218–246, 10.1177/0278364912467486.

[9] M. Rubenstein, A. Cornejo, and R. Nagpal, "Programmable self-assembly in a thousand-robot swarm." Science 15 Aug 2014: Vol. 345, Issue 6198, pp. 795-799, 10.1126/science.1254295

[10] Qu.J. Jinhong, and K.R. Oldham, "Multiple-Mode Dynamic Model for Piezoelectric Micro-Robot Walking." ASME. International Design Engineering Technical Conferences and Computers and Information in Engineering Conference, Volume 4: 21st Design for Manufacturing and the Life Cycle Conference; 10th International Conference on Micro- and Nanosystems 2016, :V004T08A023, 10.1115/DETC2016-59621.

[11] D. Vogtmann, R.S. Pierre, and S. Bergbreiter, "A 25 MG MAGNETICALLY ACTUATED MICROROBOT WALKING AT > 5 BODY LENGTHS/SEC." Proc. of the IEEE 30th International Conference on Micro Electro Mechanical Systems, Las Vegas, NV, USA, 2017, pp. 179-182, DOI: 10.1109/MEMSYS.2017.7863370.

[12] J. Rahmer, C. Stehning, and B. Gleich, "Spatially selective remote magnetic actuation of identical helical micromachines." Sci. Robot. 2017 2, eaal2845, 10.1126/scirobotics.aal2845.

[13] J.J. Abbott, Z. Nagy, F. Beyeler, and B.J Nelson, "Robotics in the Small, Part I: Microbotics." IEEE Robotics & Automation Magazine, 14(2), 2007 pp. 92-103, 10.1109/MRA.2007.380641.

[14] K. Cho, and R. Wood, "Biomimetic robots." Springer International Publishing, Cham, Switzerland, Chap. 23, 2016, ISBN: 978-3-319-32552-1

[15] R.S. Fearing, "Powering 3 Dimensional Microrobots: Power Density Limitations." Proc. of the IEEE International Conference on robotics and automation, Tutorial on Micro Mechatronics and Micro Robotics. 1998

[16] D.J. Bell, T.J. Lu, N.A. Fleck, and S.M. Spearing, "MEMS actuators and sensors: observations on their performance and selection for purpose." Journal of Micromechanics and Microengineering, 15(7), 2005, pp. S153-S164, 10.1088/0960-1317/15/7/022.

[17] K. Saito, K. Maezumi, Y. Naito, T. Hidaka, K. Iwata, Y. Okane, H. Oku, M. Takato, and F. Uchikoba, "Neural Networks Integrated Circuit for Biomimetics MEMS Microrobot Robotics." 3, 2014, pp. 235-246, 10.3390/robotics3030235

[18] D. Tanaka, Y. Uchiumi, S. Kawamura, M. Takato, K. Saito, F. Uchikoba, "Four-leg independent mechanism for MEMS microrobot. Artificial Life and Robotics." September 2017, Volume 22, Issue 3, pp 380–384, 10.1007/s10015-017-0365-2

[19] R. Yeh, S. Hollar, and K.S.J. Pister, "Single mask, large force and large displacement electrostatic linear inchworm motors." J. Microelectromech. Syst. Vol. 11 no. 4 2002, pp. 330-336, 10.1109/JMEMS.2002.800937.

[20] I. Penskiy, and S. Bergbreiter, "Optimized electrostatic inchworm motors using a flexible driving arm." Journal of Micromechanics and Microengineering, 23(1), 2012, pp. 1-12, 10.1088/0960-1317/23/1/015018.

[21] D.S. Contreras, D.S. Drew, and K.S.J. Pister, "First steps of a millimeter-scale walking silicon robot." Proc. of the 19th Int. Conference on Solid-State Sensors, Actuators and Microsystems, Kaohsiung, Taiwan, 2017.

[22] I. Mori, M. Kubota, E. Lebrasseur, and Y. Mita, "Remote power feed and control of MEMS with 58 V silicon photovoltaic cell made by a CMOS post-process dry release and device isolation method." Symposium on Design, Test, Integration & Packaging of MEMS/MOEMS (DTIP2014), April 1-4, Cannes, France, 10.1109/DTIP.2014.7056670.

[23] Y. Takeshiro, Y. Okamoto, and Y. Mita, "Mask-programmable on-chip photovoltaic cell array." Proc. of the Power MEMS 2017, November 14-17, Kanazawa, Japan, pp. 596-597.